Journal of Catalysis 257 (2008) 233–243

Contents lists available at ScienceDirect

Journal of Catalysis

www.elsevier.com/locate/jcat

Synthesis, characterization, and catalytic activity of anionic iron(III) porphyrins intercalated into layered double hydroxides

Matilte Halma [a], Kelly Aparecida Dias de Freitas Castro [a], Christine Taviot-Gueho [c], Vanessa Prévot [c], Claude Forano [c], Fernando Wypych [b], Shirley Nakagaki [a,*]

[a] Laboratory of Bioinorganic Chemistry and Catalysis, Department of Chemistry, Federal University of Paraná, UFPR, P.O. Box 19081, Curitiba, Paraná 81531-990, Brazil
[b] Solid State Chemistry Laboratory, LQES, Department of Chemistry, Federal University of Paraná, UFPR, P.O. Box 19081, Curitiba, Paraná 81531-990, Brazil
[c] Laboratoire des Matériaux Inorganiques, UMR CNRS 6002, Université Blaise Pascal, 63177 Aubière Cedex, France

ARTICLE INFO

Article history:
Received 7 March 2008
Revised 29 April 2008
Accepted 30 April 2008
Available online 13 June 2008

Keywords:
Intercalation
Porphyrins
Layered double hydroxides
Catalysis
Oxidation

ABSTRACT

The first generation free-base anionic porphyrin $[H_2(TSPP)]^{4-}$, its iron(III) porphyrin $[Fe(TSPP)]^{3-}$, and the second generation anionic complexes $[Fe(TDFSPP)]^{3-}$ and $[Fe(TDCSPP)]^{3-}$ were intercalated into the layered double hydroxide Zn_nAl-LDH ($n = 2$, 4 or 5) by coprecipitation at constant pH. The materials were characterized by X-ray powder diffraction, UV/visible spectroscopy in glycerin mull, attenuated total reflectance Fourier transform infrared spectroscopy, and electron paramagnetic resonance. Results revealed that the coprecipitation method led to intercalation of the free-base porphyrin and the iron(III) porphyrins between the Zn_nAl-LDH layers. The materials were used as catalysts in the oxidation of cyclooctene, cyclohexene, and cyclohexane by iodosylbenzene. The catalytic activity of [Fe(TDCSPP)]-Zn_2Al-LDH was higher than that of the homogeneous $[Fe(TDCSPP)]^{3-}$, but the opposite effect was observed in the case of [Fe(TDFSPP)]-Zn_2Al-LDH. Although $[Fe(TDFSPP)]^{3-}$ and $[Fe(TDCSPP)]^{3-}$ are structurally similar, their intercalation into Zn_2Al-LDH likely results in different chemical environments, leading to distinct catalytic activities.

1. Introduction

Bioinspired oxidation catalysts based on metalloporphyrins have been extensively studied over the past 3 decades. These compounds are well known for their ability to catalyze the oxidation of various substrates under mild conditions, including inert molecules such as alkanes. For this reason, they are considered mimics of the cytochrome P450-dependent monooxygenases [1–5]. Metalloporphyrins can be used in homogeneous solution or immobilized on solid matrices, such as organic amorphous polymers and crystalline inorganic materials. Examples of the latter supports include silica [6–9], fibrous chrysotile [2], zeolite [10–12], and clays from the smectite group (montmorillonite) [13,14] (among others [15–25]). Immobilization of metalloporphyrins carrying electron-withdrawing substituents, the so-called "second generation" metalloporphyrins [26], on inorganic supports leads to efficient and selective catalysts for hydrocarbon oxidation. The inorganic support confers shape-selectivity to the metalloporphyrin, thus promoting a special environment for the reaction between the substrate and the active catalytic species, which would not occur in homogeneous medium [1,7–9,22,23,27]. Immobilization prevents metalloporphyrin aggregation and/or bimolecular self-destruction, thus avoiding deactivation of the metalloporphyrin catalytically active species. In addition, metalloporphyrin immobilization facilitates catalyst recovery and reuse [18].

Layered double hydroxides (LDHs) have high surface area and good anion-exchange and expansion properties, which make them promising matrices for the immobilization of anionic metalloporphyrins. Metalloporphyrins can either intercalate between the layers or bind to the surface of the support [17,19]. In this work, the second-generation iron(III) porphyrins $[Fe(TDFSPP)]^{3-}$ and $[Fe(TDCSPP)]^{3-}$ (Fig. 1) were intercalated in the interlayer space of Zn_nAl-LDH by coprecipitation at constant pH. The catalytic activity of [Fe(TDFSPP)]-Zn_nAl-LDH and [Fe(TDCSPP)]-Zn_nAl-LDH in the oxidation of cyclooctene, cyclohexane, and cyclohexene by iodosylbenzene also was investigated, and the results were compared with those obtained with other iron(III) porphyrin systems described in the literature. [H_2(TSPP)]-Zn_nAl-LDH and [Fe(TSPP)]-Zn_nAl-LDH were also prepared for comparison purposes. [H_2(TSPP)]-Zn_nAl-LDH and [Fe(TSPP)]-Zn_nAl-LDH were subjected to hydrothermal treatment, which led to improved crystallinity and allowed for deeper structural characterization.

* Corresponding author. Fax: +55 41 3361 3186.
E-mail address: shirley@quimica.ufpr.br (S. Nakagaki).

0021-9517/$ – see front matter
doi:10.1016/j.jcat.2008.04.026

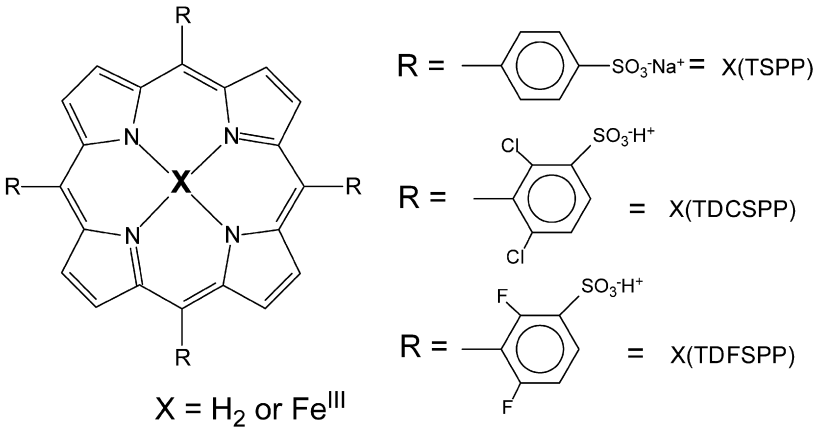

Fig. 1. Schematic representation of iron(III) porphyrins.

2. Experimental

2.1. Materials

All solvents and reagents were commercial grade (Aldrich, Merck, Fluka), unless stated otherwise. Authentic samples of the alcohols, ketones, and epoxides that could be produced in the oxidation reactions were purchased at their highest commercial purity grade (Aldrich) and used as received. The substrates cyclooctene, cyclohexene, and cyclohexane were stored at 5 °C and purged with argon before use. After the experiments, all reagents were discarded in an appropriate container for later treatment and reuse when possible, or for final disposal.

2.1.1. Porphyrins

Reagent-grade free-base porphyrin H_2(TSPP) [5,10,15,20-tetrakis(4-sulfonatophenyl)porphyrin] was purchased from Aldrich and used without purification. UV/vis data H_2(TSPP) (deionized water): 421 nm ($\varepsilon = 2.7 \times 10^5$ L mol^{-1} cm^{-1}). The second-generation free-base porphyrins H_2(TDFSPP); [5,10,15,20-tetrakis(2,6-difluoro-3-sulfonatophenyl)porphyrin] and H_2(TDCSPP); [5,10,15,20-tetrakis-(2,6-dichoro-3-sulfonatophenyl)porphyrin]; were synthesized and purified as described previously. The anionic tetra charges were omitted for all free-base porphyrins for simplification (Fig. 1) [25,28,29].

2.1.2. Iron(III) porphyrins

Iron(III) porphyrin (FePs) were obtained by iron insertion into the free-base porphyrin ligands using ferrous chloride tetrahydrate in dimethylformamide (DMF), as described by Adler and Longo [30,31]. Purification of the FePs was performed by column chromatography on Sephadex, using deionized water as an eluent. The products were characterized by UV–vis and EPR spectroscopy. Data were consistent with those of the compound expected after the iron insertion reaction. UV/vis data: [Fe(TSPP)Cl] (deionized water) 394 nm ($\varepsilon = 2.4 \times 10^4$ L mol^{-1} cm^{-1}), [Fe(TDFSPP)Cl] (deionized water) 394 nm ($\varepsilon = 3.7 \times 10^4$ L mol^{-1} cm^{-1}), and [Fe(TDCSPP)Cl] (deionized water) 390 nm ($\varepsilon = 1.7 \times 10^4$ L mol^{-1} cm^{-1}).

2.1.3. Iodosylbenzene (PhIO)

PhIO was obtained through hydrolysis of iodosylbenzene diacetate, as described previously [32,33]. Purity was checked periodically by iodometric assay.

2.2. Intercalation of [H_2(TSPP)], [Fe(TSPP)], [Fe(TDFSPP)], and [Fe(TDCSPP)] into Zn_nAl-LDH

The solids [H_2(TSPP)]-Zn_nAl-LDH, [Fe(TSPP)]-Zn_nAl-LDH, [Fe(TDFSPP)]-Zn_nAl-LDH, and [Fe(TDCSPP)]-Zn_nAl-LDH were prepared by coprecipitation at constant pH, adapted for the preparation of small quantities of material. Toward this end, an aqueous solution containing $AlCl_3$ and $ZnCl_2$ and another aqueous solution containing NaOH were simultaneously added to a container (see Table 1 for details on the various $AlCl_3$, $ZnCl_2$ and NaOH concentrations used in the procedure). The volume of added NaOH was monitored via a pH electrode immersed in the reagent solution, so as to maintain the pH of the coprecipitation reaction at 7.5 ± 0.2. The average flow rate of the solution containing $AlCl_3$ and $ZnCl_2$ was obtained by dividing the transferred solution volume by the time. The mixture containing NaOH, $AlCl_3$, and $ZnCl_2$ was then slowly added to the free-base porphyrin or to a FeP solution (see Table 1 for details on concentration) under nitrogen atmosphere. The concentration of the free-base porphyrin or the FeP in the solution corresponded to fourfold the number of mol required for the exchange reaction stoichiometry. Addition of the NaOH, $AlCl_3$, and $ZnCl_2$ solution to the free-base porphyrin or FeP was completed within 6 h, and the mixture was left to age at room temperature for 2 days.

Table 1
Conditions of the porphyrins/LDH coprecipitation at constant pH

Solid	[$M^{2+} + M^{3+}$] and [NaOH] (mol/L)	[Porphyrin] or [iron(III) porphyrin] (mol/L)	V of salts (mL)	Time (min)
[H_2(TSPP)]-Zn_2Al-LDH	0.100	0.012	2.57	371
[H_2(TSPP)]-Zn_4Al-LDH	0.125	0.014	2.54	369
[H_2(TSPP)]-Zn_5Al-LDH	0.125	0.012	3.32	480
[Fe(TSPP)]-Zn_2Al-LDH	0.100	0.017	2.48	360
[Fe(TSPP)]-Zn_4Al-LDH	0.125	0.013	2.47	328
[Fe(TDFSPP)]-Zn_2Al-LDH	0.100	0.004	0.70	310
[Fe(TDCSPP)]-Zn_2Al-LDH	0.100	0.003	0.62	292

After the intercalation reaction, [H_2(TSPP)]-Zn_nAl-LDH, [Fe(TSPP)]-Zn_nAl-LDH, [Fe(TDFSPP)]-Zn_2Al-LDH, and [Fe(TDCSPP)]-Zn_2Al-LDH were washed with deionized water and recovered by centrifugation. The combined washing solutions were stored and analyzed by UV–vis spectroscopy, to quantify any free-base porphyrin or FeP that might have leached from the matrix during the dispersion-centrifugation process. The obtained green solids were air-dried, and the following [H_2(TSPP)]/solid and FeP/solid loadings were obtained: [H_2(TSPP)]-Zn_2Al-LDH = 8.8 × 10^{-4} mol free-base porphyrin/g solid; [H_2(TSPP)]-Zn_4Al-LDH = 1.1 × 10^{-3} mol free-base porphyrin/g solid; [H_2(TSPP)]-Zn_5Al-LDH = 7.7 × 10^{-4} mol free-base porphyrin/g solid; [Fe(TSPP)]-Zn_2Al-LDH = 8.9 × 10^{-4} mol iron(III) porphyrin/g solid; [Fe(TSPP)]-Zn_4Al-LDH = 7.9 × 10^{-4} mol iron(III) porphyrin/g solid; [Fe(TDFSPP)]-Zn_2Al-LDH = 1.1 × 10^{-3} mol iron(III) porphyrin/g solid, and [Fe(TDCSPP)]-Zn_2Al-LDH = 1.2 × 10^{-3} mol iron(III) porphyrin/g solid.

To improve the crystallinity of the materials prepared as above and to gain further insight into their structural arrangement, the [H_2(TSPP)]-Zn_2Al-LDH, [H_2(TSPP)]-Zn_4Al-LDH, [Fe(TSPP)]-Zn_2Al-LDH, and [Fe(TSPP)]-Zn_4Al-LDH samples were submitted to hydrothermal treatment. The resulting products were denoted [H_2-(TSPP)]-Zn_2Al-LDH_{Hyd}, [H_2(TSPP)]-Zn_4Al-LDH_{Hyd}, [Fe(TSPP)]-Zn_2Al-LDH_{Hyd}, and [Fe(TSPP)]-Zn_4Al-LDH_{Hyd}, respectively. Toward this end, 50 mg of the coprecipitated phases were suspended in 25 mL of deionized water in a Teflon inner vessel (30 mL) placed in a stainless steel outer autoclave, and the solids were kept there at 120 °C for 72 h under autogeneous pressure.

2.3. Oxidation of cyclooctene, cyclohexene and cyclohexane by PhIO catalyzed by anionic FePs in homogeneous medium or intercalated into Zn_nAl-LDH

The oxidation reactions were carried out in a thermostatic glass reactor (2 mL) equipped with a magnetic stirrer, placed inside a dark chamber [15,18]. In the case of the Zn_nAl-LDH-intercalated FePs (heterogeneous catalysis), the solid catalyst and iodosylbenzene (in an FeP/PhIO molar ratio 1:10) were suspended in dichlorometane/acetonitrile 1:1 v/v mixture (0.350 mL) and degassed with argon for 15 min. The substrate (cyclohexane, cyclooctene, or cyclohexene) was then added to the glass reactor at an FeP/substrate molar ratio of 1:1000, and the oxidation reaction was performed for 1 h under magnetic stirring. Sodium sulfite was added to eliminate any excess iodosylbenzene and to quench the reaction. The reaction products were separated from the solid catalyst (heterogeneous catalysis) by exhaustive washing and centrifugation of the FeP-Zn_nAl-LDH catalyst with a dichlorometane/acetonitrile 1:1 v/v mixture. The combined washing solutions were analyzed by capillary gas chromatography. The products were identified by comparing their retention times with those of authentic samples. Product yields were determined by the internal standard method. Control reactions were carried out with the chlorine-intercalated Zn_nAl-LDH containing no FeP and with a solution blank setup with no solid. A similar procedure was adopted when iron(III) porphyrins were used as homogeneous catalyst.

2.4. Instruments

X-ray powder diffraction patterns (XRPD) were recorded on a Philips X-Pert Pro diffractometer equipped with an X-Celerator detector using Cu$K\alpha_1/\alpha_2$ radiation. Data were collected between 2° and 70° (2θ, with a step size of 0.03° and a counting time of 100 s/step). The cell parameters were determined from peak profile analysis using the Fullprof program (Full Pattern Matching) [34]. Before the analyses, the samples were mixed with 10 wt% of a polycrystalline silicon standard, to obtain accurate unit cell parameters for the Zn_nAl-LDH-containing free-base porphyrin or FeP. The Lorentzian component of the TCH pseudo-Voigt profile function was modeled using a linear combination of spherical harmonics to take into account the anisotropic broadening due to anisotropic size effects [34,35]. A Rietveld refinement was carried out on the [Zn_2Al-Cl] reference sample (LDH containing no intercalated complexes) starting from the model given in the literature [36].

UV–visible spectra (UV/vis) were obtained with a NICOLET evolution 500 Diode Array spectrophotometer, using solid samples dispersed in glycerol mulls placed between two quartz plates. Electron paramagnetic resonance (EPR) of the supported metalloporphyrin systems in the solid state was performed on a Bruker ESP 300E spectrometer operating at the X-band (approximately 9.5 GHz), at 77 K, using liquid N_2. Attenuated total reflectance Fourier transform infrared (ATR/FTIR) spectra were recorded on a NICOLET 5700 equipment in the 4000–400 cm^{-1} range, with a resolution of 8 cm^{-1} and accumulation of 120 scans. Products from the catalytic oxidation reactions were identified using a Shimadzu CG-14B gas chromatograph equipped with a flame ionization detector and a DB-WAX capillary column (J & W Scientific).

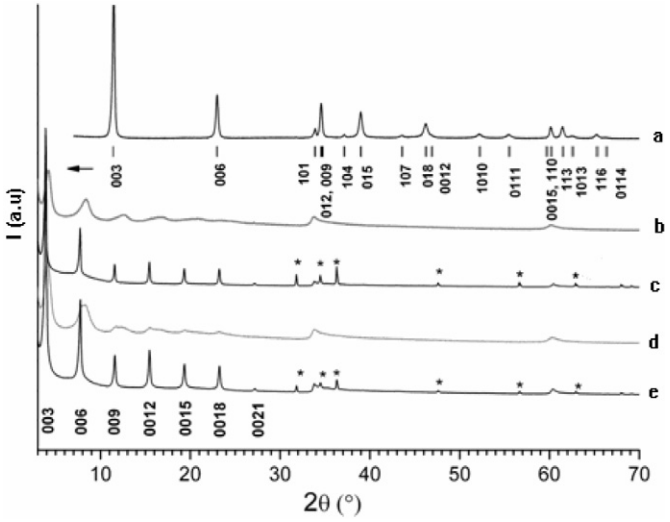

Fig. 2. X-ray powder diffraction patterns of [Zn_2Al-Cl] LDH (a), [H_2(TSPP)]-Zn_4Al-LDH before (b) and after the hydrothermal treatment (c) and [H_2(TSPP)]-Zn_2Al-LDH before (d) and after the hydrothermal treatment (e). Ticks and labels give the Bragg reflections in the space group R-3m and peaks noted with an asterisk correspond to ZnO.

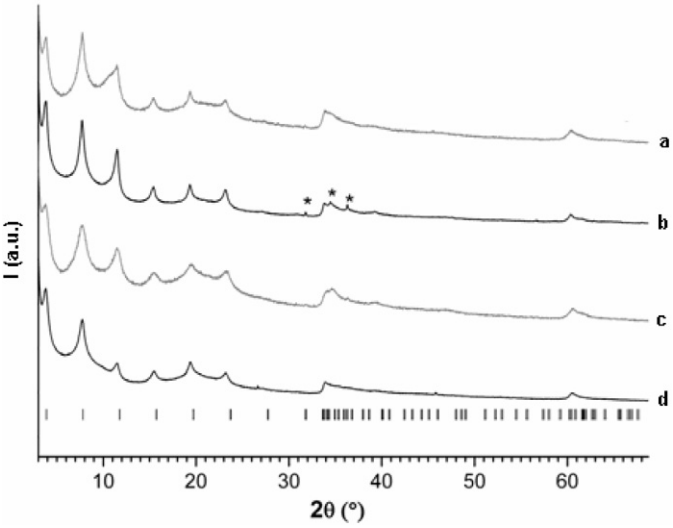

Fig. 3. X-ray powder diffraction patterns in the 2θ range 2°–70° of [Fe(TSPP)]-Zn_4Al-LDH before (a) and after the hydrothermal treatment (b) and [Fe(TSPP)]-Zn_2Al-LDH (c) and after hydrothermal treatment (d). Ticks give the Bragg reflections in the space group R-3m and peaks noted with an asterisk correspond to ZnO.

3. Results and discussion

3.1. Characterization of the Zn_nAl-LDH-intercalated FeP catalysts

3.1.1. X-ray powder diffraction

All of the materials prepared in this work displayed XRPD patterns typical of Zn_nAl-LDH materials (Figs. 2–4), yet the diffraction patterns were broad compared with those for the [Zn_2Al-Cl] pristine material containing no free-base porphyrin or FeP. This is likely due to the simultaneous effects of small coherent domain size and structural disorder following porphyrin intercalation. The

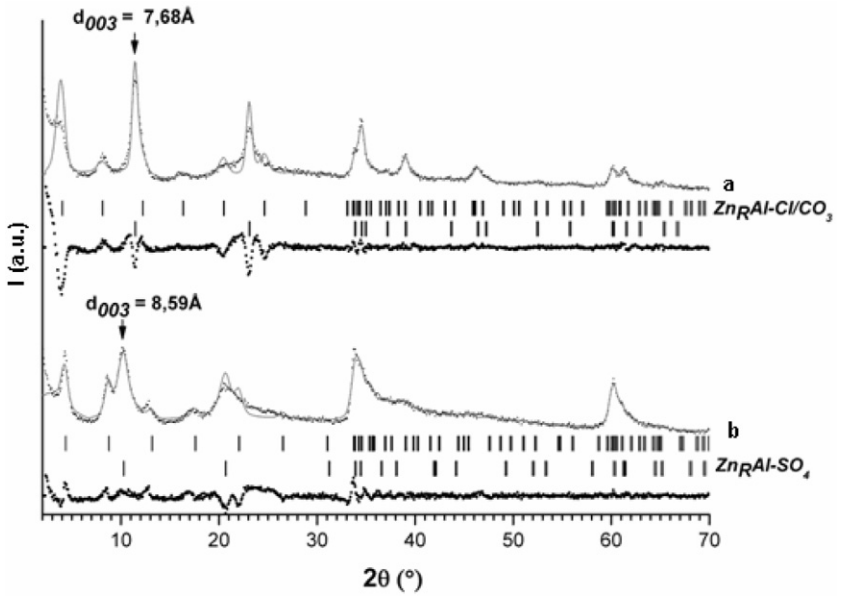

Fig. 4. Results of the profile analysis of XRPD patterns for [Fe(TDCSPP)]-Zn_2Al-LDH (a) and [Fe(TDFSPP)]-Zn_2Al-LDH (b): experimental X-ray diffraction (dots) and calculated (line).

Table 2
Refined cell parameters and microstructural data for porphyrin-LDH materials

LDH phases	Cell parameters (Å)	In-plane (110) and out–of-plane (001) coherence lengths (Å)	R_{calc}/R_{theo}	S_o (Å^2/e) $= \sqrt{3a^2/2x}$
Zn_2Al-Cl	$a = 3.07526(2)$			
	$c = 23.2459(8)$; $d_{003} = 7.749$	1950/460		
[H_2(TSPP)]-Zn_2Al-LDH	$a = 3.077(2)$			
	$c = 66.9(3)$; $d_{003} = 22.3$	115/75	2.07/2.0	25.15
[H_2(TSPP)]-Zn_4Al-LDH	$a = 3.082(1)$			
	$c = 64.5(1)$; $d_{003} = 21.5$	–	2.29/4.0	27.06
[Fe(TSPP)]-Zn_2Al-LDH	$a = 3.071(3)$	–		
	$c = 68.5(2)$; $d_{003} = 22.8$		1.82/2.0	23.07
[Fe(TSPP)]-Zn_4Al-LDH	$a = 3.075(2)$	–		
	$c = 69.3(2)$; $d_{003} = 23.1$		1.98/4.0	24.37
[H_2(TSPP)]-Zn_2Al-LDH_{Hyd}	$a = 3.0620(2)$	680/505		
	$c = 68.98(4)$; $d_{003} = 22.99$		1.53/2	20.55
[H_2(TSPP)]-Zn_4Al-LDH_{Hyd}	$a = 3.0618(7)$	–		
	$c = 68.99(1)$; $d_{003} = 22.99$		1.52/4	20.50
[Fe(TSPP)]-Zn_2Al-LDH_{Hyd}	$a = 3.063(1)$	–		
	$c = 68.86(6)$; $d_{003} = 22.95$		1.56/2	20.78
[Fe(TSPP)]-Zn_4Al-LDH_{Hyd}	$a = 3.063(1)$	–		
	$c = 69.23(5)$; $d_{003} = 23.07$		1.56/4	20.78
[Fe(TDCSPP)]-Zn_2Al-LDH	$a = 3.073(2)$	–		
	$c = 64.9(1)$; $d_{003} = 21.6$			
[Fe(TDFSPP)]-Zn_2Al-LDH	$a = 3.069(2)$	–		
	$c = 60.49(5)$; $d_{003} = 20.16$			

lower signal-to-noise ratio seen in the Fe(TSPP)-containing samples may be attributed in part to iron fluorescence. Diffraction peaks are indexed as in the case of [Zn_2Al-Cl], on a hexagonal unit cell with the space group R-3m. The cell parameters gathered in Table 2 were obtained from profile peak analysis.

The intercalation of porphyrin complexes into the LDH led to strong enlargement of the basal distance d_{003}, as seen from the displacement of the 003 reflection toward low 2θ angles. The d_{003} values of 20–23 Å suggest a perpendicular arrangement of the porphyrin ring with respect to the hydroxide layer (discussed below). As evidenced from the position of the reflection markers at the bottom of the XRPD patterns, the [H_2(TSPP)]-Zn_2Al-LDH, [H_2(TSPP)]-Zn_4Al-LDH, [Fe(TSPP)]-Zn_2Al-LDH, and [Fe(TSPP)]-Zn_4Al-LDH samples are single-phase materials (Figs. 2 and 3), whereas [Fe(TDFSPP)]-Zn_2Al-LDH and [Fe(TDCSPP)]-Zn_2Al-LDH are not pure samples (Fig. 4). The impurities in the latter consist of Zn_2Al-LDH phases intercalated with inorganic anions. For [Fe(TDCSPP)]-Zn_2Al-LDH, the basal distance $d_{003} \sim 7.7$ Å can be ascribed to either chloride (competition with chloride metallic salts) or carbonate anions (contamination from atmospheric CO_2). As for the [Fe(TDFSPP)]-Zn_2Al-LDH sample, the additional diffraction peaks may be attributed to the [Zn_RAl-SO_4] phase with $d_{003} \sim 8.6$ Å; however, the source of sulfate anions is questionable and could lie on the porphyrin sulfonation process. Using a correlation between the cell parameter a and the Zn/Al molar ratio R established elsewhere for the [Zn_RAl-Cl] series, an R value close to 2 was obtained in all cases, even for samples prepared with a Zn/Al ratio of 4. Therefore, it can be inferred that the intercalated porphyrins are partly responsible for the Zn/Al ratio, that is, the charge density of the hydroxide layers.

To improve the crystallinity of the samples and gain better insight into the porphyrin-Zn_nAl-LDH structures, the single

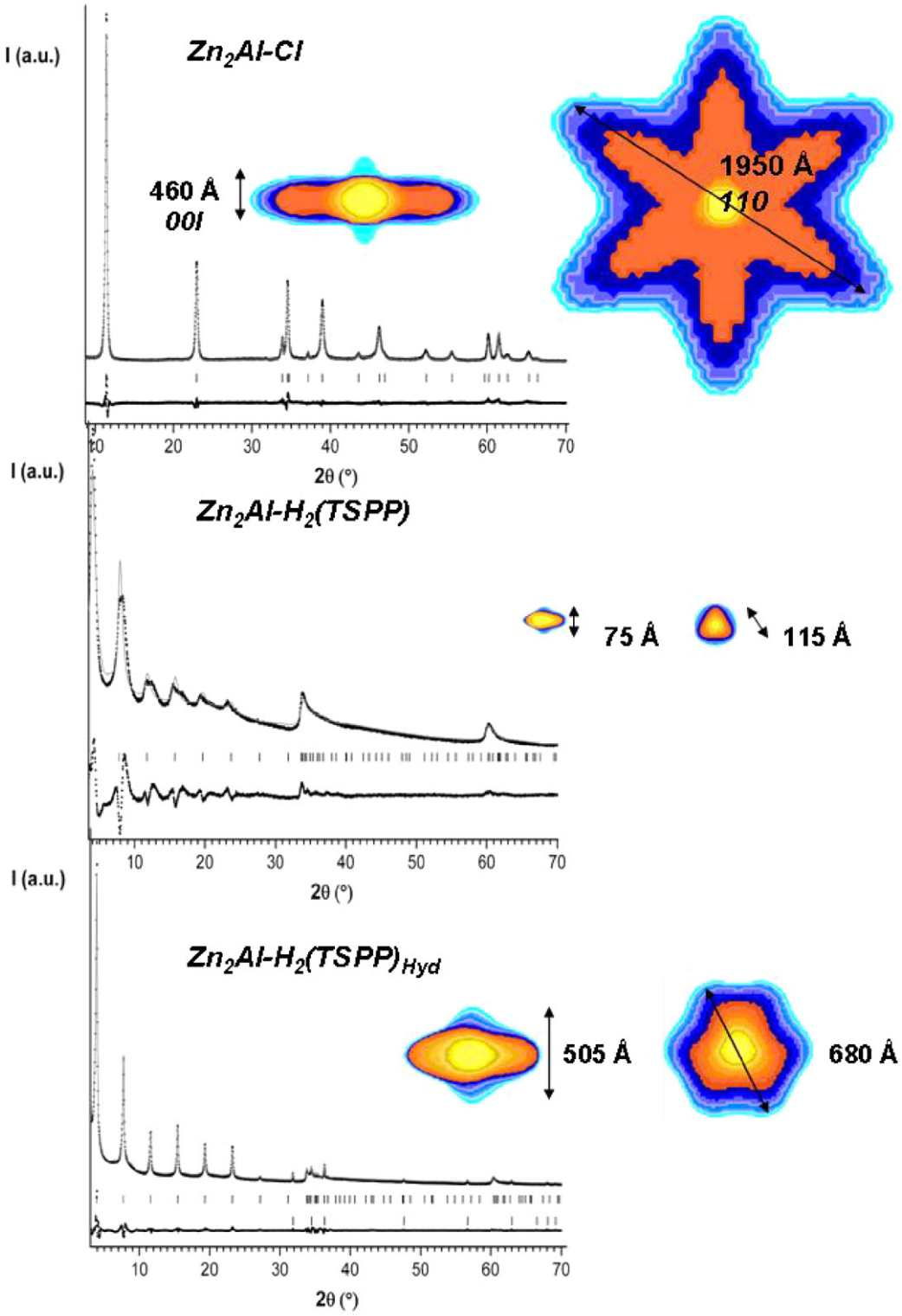

Fig. 5. Results of the analysis of the XRPD profile of Rietveld refinement [Zn_2Al-Cl] (a), [H_2(TSPP)]-Zn_2Al-LDH before (b) and after hydrothermal treatment (c). Experimental X-ray diffraction (dots) and calculated (line). The insets show the average apparent shape of the crystallite coherent domains.

phases [H_2(TSPP)]-Zn_2Al-LDH, [H_2(TSPP)]-Zn_4Al-LDH, [Fe(TSPP)]-Zn_2Al-LDH, and [Fe(TSPP)]-Zn_4Al-LDH were subjected to a post-synthesis hydrothermal treatment. The narrowing of the diffraction peaks suggests a net improvement in the crystallinity of the [H_2(TPPS)]-containing materials (Figs. 2 and 3). The results of the full-pattern matching refinements of [H_2(TSPP)]-Zn_2Al-LDH and [H_2(TSPP)]-Zn_2Al-LDH_{Hyd} and the Rietveld refinement of [Zn_2Al-Cl] are given in Fig. 5.

Good profile refinements were obtained by assuming that the anisotropic broadening is due to size effects, which allowed determination of both the size and the average form of the coherent domains. It was possible to reconstruct the apparent sizes along different directions from the refined profile coefficients. Hexagonal platelet coherent domains were obtained, in total agreement with the hexagonal platelet-like morphology of Zn_nAl-LDH materials. The size of the coherent domains of [H_2(TSPP)]-Zn_2Al-LDH

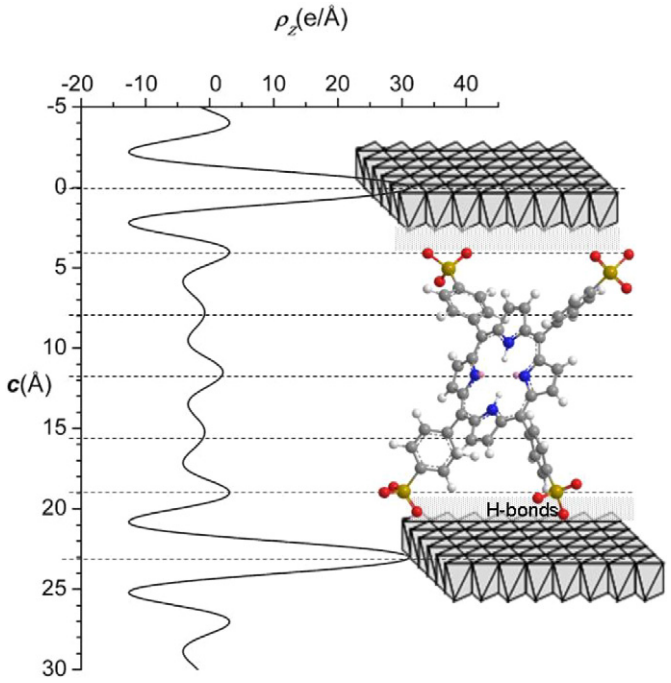

Fig. 6. One-dimensional electron density $\rho(z)$ projection along the c-axis for [H_2-(TSPP)]-Zn_2Al-LDH_{hyd} and the corresponding structural model.

(in-plane dimension of 115 Å and thickness of 75 Å) was found to be 6-fold larger after the solid underwent hydrothermal treatment (in-plane dimension of 680 Å and thickness of 450 Å), and the same effect on particle size can be assumed. For [Zn_2Al-Cl], the size of the coherent domains (195/45 nm) is associated with an average particle size of 500 nm (i.e., in the submicrometric range). The broad features displayed by the materials containing FeP suggest the presence of very small particles, certainly in the nanometer range (<100 nm). On the other hand, the Zn/Al ratio deduced from the value of the cell parameter a was found to decrease and converge to 1.5 on hydrothermal treatment for all of the samples. The simultaneous formation of ZnO was observed in the XRPD pattern, and more of this oxide was present in the Zn_4Al-samples than in the Zn_2Al-samples. Although further characterization is needed to clarify this phenomenon, this result strongly suggests that the hydrothermal process proceeds via a dissolution, precipitation, and crystallization mechanism. Under autogeneous pressure (∼2 bars), dissociation of water at 120 °C is increased, and the pH of the solution is slightly acidic. Based on the Pourbaix diagrams of these species, only Zn_RAl-LDH with low Zn/Al molar ratio can be precipitated in these conditions.

The relative large number of basal reflections observed for [H_2(TSPP)]-Zn_2Al-LDH_{Hyd} (up to seven harmonics), related to the large size of the intercalated porphyrin, allowed us to probe the structure of the interlayer space projected on the c-axis via Fourier transform analysis. The electron density was calculated from the known structure of the hydroxide layer, assuming a weak contribution from the interlayer portion to the total scattering. The 1-D electron density map of [H_2(TSPP)]-Zn_2Al-LDH_{Hyd} (Fig. 6) $\rho(Z)$ gave rise to two strong peaks at $d = 0$ and 23.0 Å, because the hydroxide layers contain the metal cations. Five additional peaks of lower electron density, due to the porphyrin molecule, were observed between the layers. On comparison with the dimensions of the porphyrin molecule, which is a parallelepiped of about 16.0 × 15.8 × 4.3 Å as obtained from steric energy minimization using the MM2 method [36], we propose a perpendicular arrangement of the porphyrin against the hydroxide layers, in agreement with previous studies [17].

The sulfonate groups led to maxima at the outer parts of the interlayer space, that is, $d = 4.0$ and 19.0 Å. This position is coherent with the existence of hydrogen-bonding interactions between these sulfonate groups and the hydroxylated layers. The central maximum is attributed to the four inner nitrogen atoms of the porphyrin ring, whereas the intermediate peaks of lower intensity spaced approximately 7.6 Å from each other arise from the opposite phenyl groups. With such an orientation, the porphyrin molecule displayed a surface area of ∼17.3 $Å^2$ per unit charge, largely satisfied by the host lattice for a Zn/Al ratio of 2 (24.8 $Å^2/e^-$), and in far better accordance with $R = 1.5$ (20.3 $Å^2/e^-$). In the latter case, a slightly inclined orientation of the porphyrin, achieved by increasing the surface required by the porphyrin, should lead to exact matching between the Zn_2Al-LDH host and the porphyrin guest, thus causing an optimization of the electrostatic interactions. Yet the 1-D plot does not allow us to distinguish between a perpendicular or a slightly oriented arrangement.

A similar perpendicular orientation is proposed for all the other materials, including those containing FeP. The slight variations observed in the d_{003} values must be first ascribed to the different crystallinity of these materials and/or different interlayer water contents. Nevertheless, in [Fe(TDFSPP)]-Zn_2Al-LDH and [Fe(TDCSPP)]-Zn_2Al-LDH, the substitution of the two *ortho* hydrogen atoms on the *meso*phenyl group by fluorine or chlorine certainly had an effect on gallery height. In the particular case of the chlorine-substituted derivative [Fe(TDCSPP)]-Zn_2Al-LDH, the d_{003} of 21.6 Å suggests that intramolecular steric hindrance forced the rotation of both the phenyl and the sulfonate groups, leading to rearrangement of the porphyrin anions to optimize the guest–host interactions.

3.1.2. UV–visible absorption spectra

The presence of FeP in the Zn_nAl-LDH matrix also was confirmed by UV–visible spectra of the solids in glycerin mull (Fig. 7). Two sets of absorption bands are seen in the UV–visible spectra of porphyrins. The Soret band is characterized by a large absorption coefficient and lies in the 400–450 nm range. A second set of weaker bands, the Q bands, occurs between 450 and 700 nm [17]. Our measurements suggested that no demetallation (characterized by a blue-shift of the Soret band associated with a significant amount of free-base porphyrin [22,24]) or significant exchange of the Fe(III) ion with the support occurring during the catalyst intercalation carried out in this work [2,18]. The Soret peaks of the intercalated phases [Figs. 7b (418 nm), 7c, 7e, and 7g (414 nm)] were slightly shifted to higher wavelengths compared with those of the pure FePs [Figs. 7a (408 nm), 7d (410 nm), and 7f (414 nm)]. This behavior can be attributed to steric constraints caused by the support, which substantially distort the FeP molecule in these supported catalysts [31]. It also could be an indication that most of the FePs was intercalated between the Zn_nAl-LDH layers [18]. Peak broadening also was observed in the case of the intercalated FePs compared with the parent complexes in solution, which also can be explained by the presence of the different intermolecular interactions.

3.1.3. Electron paramagnetic resonance

Fig. 8 shows the EPR spectra of all the Zn_nAl-LDHs intercalated with the FePs. They all display a common signal in $g = 5.7$ (axial symmetry), typical of a high-spin 5/2 FeP complex [10,15,18]. There also was a slight distortion from the rhombic symmetry, as demonstrated by the signal in $g = 4.3$. The higher intensity of the signal due to axial symmetry in $g = 5.7$ suggests intercalation of the FeP between the layers of the Zn_nAl-LDH and also that no demetallation occurred during the immobilization procedure [13,14,18], as

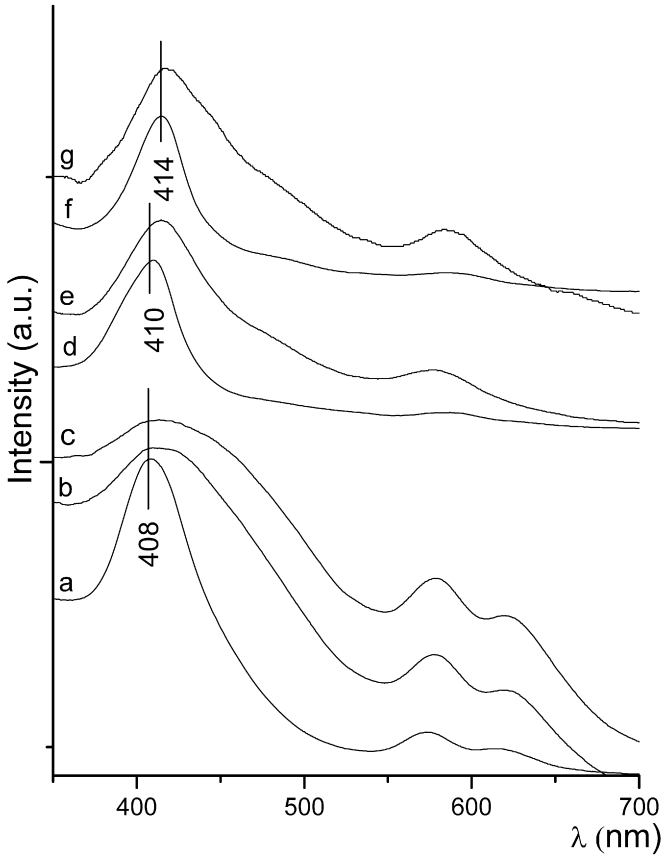

Fig. 7. UV–vis spectra of the FePs and FeP-Zn_nAl-LDHs in glycerin mull. Fe(TSPP) (a), [Fe(TSPP)]-Zn_4Al-LDH (b), [Fe(TSPP)]-Zn_2Al-LDH (c), Fe(TDFSPP) (d), [Fe(TDFSPP)]-Zn_2Al-LDH (e), Fe(TDCSPP) (f), [Fe(TDCSPP)]-Zn_2Al-LDH (g).

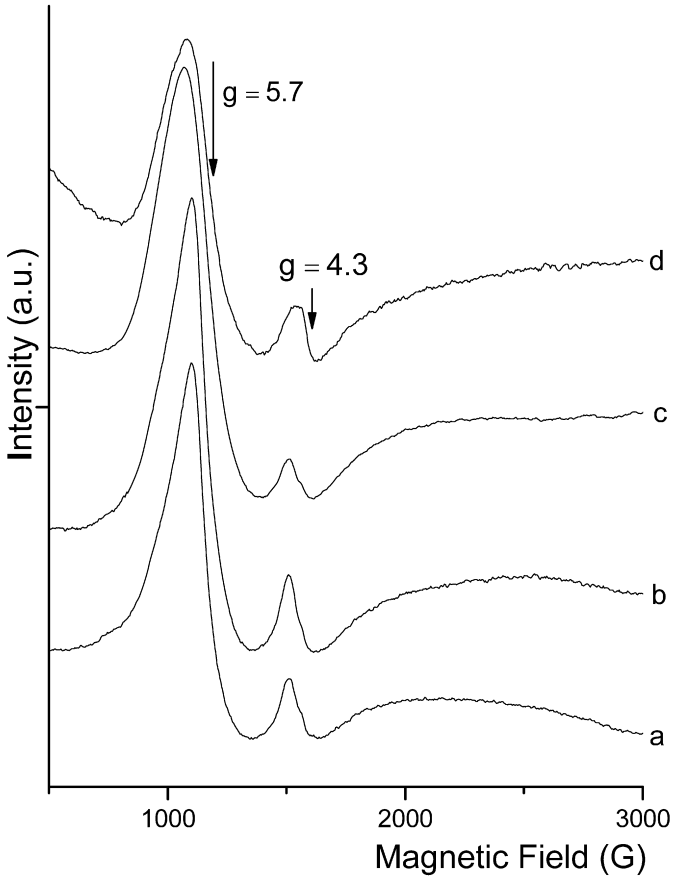

Fig. 8. EPR spectra of solid samples obtained at 77 K. [Fe(TSPP)]-Zn_2Al-LDH (a), [Fe(TSPP)]-Zn_4Al-LDH (b), [Fe(TDFSPP)]-Zn_2Al-LDH (c), [Fe(TDCSPP)]-Zn_2Al-LDH (d).

also suggested by the UV–vis data. This signal also indicates that only slight distortion of the porphyrin ring occurred on intercalation.

3.1.4. Infrared spectroscopy

Infrared spectroscopy (diffuse reflectance) was performed to provide information about the main vibrations of the porphyrin rings and the vibration bands of the Zn_nAl-LDH support (spectra not shown). The porphyrin rings displayed vibration bands in the region 1600–1370 cm^{-1}, due to νC=C phenyl and νC=N. Bands were also seen in the 1200–1020 cm^{-1} region, typical of the $\nu_{sym}S-\phi$ and $\nu_{sym}S-\phi$ symmetric and asymmetric vibrations of the $\phi-SO_3$ groups. The bands in the 720–640 cm^{-1} region are attributed to out–of-plane C–H vibrations [17,37,38]. The intercalated porphyrin rings displayed vibration bands in the same positions as the free porphyrins, indicating weak interactions between the host and guest partners. Similarly, all of the intercalated materials displayed the bands typical of the Zn_nAl-LDH matrix in the 430-cm^{-1} region, attributed to M–O and O–M–O bonds. Therefore, the layer integrity within the support was maintained despite the large basal spacing. A slight contamination of the phase with carbonate anions (likely due to the drying method used in this work), characterized by the presence of a band in 1365 cm^{-1}, also was observed.

3.2. Investigation of the catalytic activity of the intercalated FePs

The catalytic activity of all the intercalated FePs (heterogeneous catalysis) and of the parent FePs in solution (homogeneous catalysis) was investigated in the oxidation of cyclooctene, cyclohexene, and the poorly reactive alkane cyclohexane.

3.2.1. Cyclooctene

It is well known that the oxidation of cyclooctene by metalloporphyrin/PhIO systems produces epoxide as the oxidation product, with no traces of allylic alcohol or ketone. This behavior is justified by the low stability of the allyl radical intermediate transient species proposed for substrate conversion into the allylic products [39]. For this reason, cyclooctene is frequently used as a diagnostic substrate in catalytic systems involving metalloporphyrins. In the present work, we used this alkene to investigate the efficiency and stability of the immobilized anionic FePs as catalyst in alkene oxidation by PhIO. This study also provided information regarding the accessibility of the substrate and the oxidant to the iron(III) sites on the intercalated catalyst.

Table 3 (runs 1–7) characterizes the epoxidation of cyclooctene by PhIO catalyzed by the FePs either in solution or immobilized on Zn_nAl-LDH. The reproducibility of the reaction results was excellent (deviation of ca. 2%).

Control reactions using PhIO in the same reaction conditions (runs 8–10 in Table 3), in the absence of FePs (run 8) and with pristine Zn_2Al-LDH with no FeP as catalyst (runs 9 and 10), led to lower yields of oxidation product. This confirms that the catalytic activity observed in runs 1–7 was actually due to the FeP complexes.

No FeP leaching from the support was observed when excess substrate (FeP/substrate molar ratio = 1:1000) and a solvent mixture of CH_2Cl_2/CH_3CN 1:1 (v/v) was used. In addition, good quantitative epoxide yields based on PhIO (as high as 90%) were obtained within 1 h of reaction in the case of the second-generation FePs (run 7 in Table 3).

As for the more structurally simple anionic iron(III) porphyrin Fe(TSPP), a higher epoxide yield was achieved with the homoge-

Table 3
Oxidation of cyclooctene by PhIO catalyzed by iron porphyrins in solution (homogeneous catalysis) and immobilized in LDH (intercalated iron porphyrins: Fe(TSPP), Fe(TDFSPP), and Fe(TDCSPP)) (heterogeneous catalysis)[a]

Catalyst	Run	Cyclooctene oxide[a,b] (%)	FePor/ HDL (g/g)[c]	TON[f]
Fe(TSPP)	1	64		6.2
[Fe(TSPP)]-Zn_2Al-LDH	2	43	1.00	3.4
[Fe(TSPP)]-Zn_4Al-LDH	3	34	0.88	2.4
Fe(TDFSPP)	4	79		8.4
[Fe(TDFSPP)]-Zn_2Al-LDH	5	69	1.38	8.4
Fe(TDCSPP)	6	76		7.8
[Fe(TDCSPP)]-Zn_2Al-LDH	7	90	1.41	4.8
No catalyst solid[d]	8	10		
Zn_4Al-LDH[e]	9	11		
Zn_2Al-LDH[e]	10	16		

[a] Conditions: purged argon, cyclooctene/solvent mixture CH_2Cl_2:CH_3CN 1:1 (v/v) at room temperature. FeP/PhIO/substrate molar ratio = 1:10:1000.
[b] Yields obtained after 1 h of reaction, based on starting PhIO.
[c] Concentration of FeP in the Zn_nAl-LDH (g/g) calculated by UV–vis and Lambert–Beer law.
[d] Control reaction performed with PhIO and substrate without solid catalyst or FeP in solution.
[e] Control reaction using Zn_nAl-LDH without FeP as catalyst in the same conditions as the oxidation reaction described in (a).
[f] TON = turnover number: mol of product/mol of catalyst.

neous catalyst (run 1) compared with the heterogeneous counterpart (runs 2 and 3). The techniques that we used to characterize the heterogeneous catalysts proved that the FeP was confined between the layers of Zn_nAl-LDH. Fe(TSPP) between the Zn_nAl-LDH layers forms high-density pillared molecules, hindering the access of iodosylbenzene to the iron center compared with situation for the catalyst in a homogeneous medium. This hinders formation of the active oxometal species with two oxidation levels above the resting oxidative state, the so-called oxoiron(IV) porphyrin π-radical cation ($OFe^{IV}P^{\bullet+}$) [40–44], responsible for substrate oxidation. The access of the substrate cyclooctene to the heterogeneous catalyst also may be impaired compared with the situation for the homogeneous counterpart.

The Zn/Al ratio in the LDH also could be an important factor contributing to catalytic activity. The catalyst with a Zn/Al ratio of 2:1 (run 2 in Table 3) led to slightly higher epoxide yields compared with that with a Zn/Al ratio of 4:1 (run 3), even when the yield resulting from the control reaction using Zn_nAl-LDH only was deduced from the final results (runs 9 and 10). The solid with a Zn/Al ratio of 2:1 had a greater charge and consequently a higher density of FeP, which should favor the catalytic reaction.

Compared with Fe(TSPP), the second-generation anionic iron(III) porphyrins Fe(TDFSPP) and Fe(TDCSPP) led to better catalytic performance in solution. This was expected, because it is well known that the halogen groups in the porphyrin structure protect the porphyrin ring from self-oxidative destruction by an electronic inductive effect and stabilizes the intermediate catalytically active species [25].

Intercalation of the second-generation FePs into Zn_2Al-LDH results in interesting catalytic behavior. Zn_4Al-LDH was not used in this study because it was less efficient than Zn_2Al-LDH in the case of Fe(TSPP). Compared with the homogeneous system (run 4 in Table 3), the intercalated Fe(TDFSPP) (run 5 in Table 3) led to lower epoxide yields. These results suggest that Fe(TDFSPP) was intercalated between the Zn_2Al-LDH layers, making it less accessible to the reagents [20]. Because the atomic radii of the hydrogen and fluorine atoms differ only slightly, the porphyrin rings of Fe(TDFSPP) and Fe(TSPP) are expected to be of similar size. Therefore, it is reasonable to view the arrangement of these two catalytic species between the LDH layers as similar, and thus to expect the same steric effect described above for Fe(TSPP) for Fe(TDFSPP), which should hinder the access of the reactants PhIO and cyclooctene to the iron center. This steric effect should play a more significant role in the catalysis than the activating electronic effect of the fluorine atoms, explaining why the epoxide yield did not increase for Fe(TDFSPP)-Zn_2Al-LDH. This behavior is similar to that previously reported by us for the same FeP immobilized in a "house of cards" LDH structure [15].

Fe(TDCSPP)-Zn_2Al-LDH led to increased cyclooctenoxide yields (run 7 in Table 3) compared with its homogeneous counterpart (run 6 in Table 3). This change in behavior can be explained by recalling the XRPD data. Because Fe(TDCSPP)Zn_2Al-LDH had a larger basal spacing than Fe(TDFSPP)-Zn_2Al-LDH, the two *ortho*chlorine substituents in each *meso*phenyl porphyrin group should provide more space around Fe(TDCSPP), creating a larger cavity. This must favor the access of the oxidant and the substrate to the active catalytic site, thus promoting higher product yields [15,18,20].

3.2.2. Cyclohexane

Cyclohexane is a very useful substrate for investigating the efficiency of FePs as catalysts for alkane hydroxylation by iodosylbenzene (PhIO) [8,13,40,41]. Table 4 presents the results obtained from cyclohexane hydroxylation by PhIO catalyzed by the intercalated FePs studied in this work. Systems using the same catalysts immobilized on the surface of LDH [6,18] and on LDH layers arranged in a "house of cards" fashion [15] are also discussed for comparison.

When 1.1 to 1.4 mmol of substrate was used in the solvent mixture CH_3CN/CH_2Cl_2 1:1 (v/v ratio), no catalyst leaching from the support occurred, and these proportions lead to selective alcohol formation within 1 h. PhIO consumption in all the reactions was monitored by the presence of iodobenzene (PhI) in the gas chromatograph.

Differences between the porphyrin generations become more significant when cyclohexane, a substrate that is harder to oxidize compared with cyclooctene, is used (Table 4). Low catalytic yields and low alcohol/ketone selectivities are obtained when both homogeneous and immobilized Fe(TSPP) are used (runs 1–3 in Table 4). As for the second-generation anionic FePs (runs 4–7 in Table 4), the steric and electronic effects of the substituents led to more selective cyclohexane hydroxylation, and the results were far better than those obtained with homogeneous Fe(TSPP). Comparing the two second-generation iron(III) porphyrins [Fe(TDFSPP)] and [Fe(TDCSPP)] shows that the steric and electronic effects of the fluorine and chlorine atoms on the ring structures can account for the differences in the product yields. The alcohol yields were higher for the heterogeneous Fe(TDCSPP) (run 7 in Table 4) than for its homogeneous counterpart (run 6 in Table 4), demonstrating that catalyst immobilization led to improved catalytic performance. But the opposite behavior was seen for homogeneous Fe(TDFSPP) (run 4 in Table 4) and heterogeneous Fe(TDFSPP) (run 5 in Table 4). As described above, the larger radii of the two *ortho*chlorine substituents compared with those of the *ortho*fluorine substituents led to a larger basal spacing in the case of Fe(TDCSPP)-Zn_2Al-LDH, making the active site of the latter FeP better dispersed and more readily available for the reagents compared with Fe(TDFSPP)- Zn_2Al-LDH, thus resulting in higher product yields.

The catalytic yields presented here for the intercalated Fe (TDFSPP) were lower than those reported previously for the same FeP immobilized on the surface of LDHs [6,18]. Compared with the Fe(TDFSPP) catalyst immobilized on the LDH support in a "house of cards" arrangement, the catalytic results are virtually the same [15]. These comparisons suggest that access of reactants to the catalytic site has an important affect on the catalytic activity of FePs intercalated between LDH layers [6,18].

It is noteworthy that reactions using the Zn_nAl-LDH support itself without intercalated FeP did not give any hydroxylation

Table 4
Oxidation of cyclohexane and cyclohexene by PhIO catalyzed by iron porphyrins in solution (homogeneous catalysis) and immobilized in LDH (intercalated iron porphyrins: Fe(TSPP), Fe(TDFSPP), and Fe(TDCSPP)) (heterogeneous catalysis)[a]

Catalyst	Cyclohexane[a]				Cyclohexene[a,e]			
	Run	Ol (% yield)[c]	One (% yield)[d]	TON[i]	Oxide (% yield)	One (% yield)	Ol (% yield)	TON[i]
Fe(TSPP)[b]	1	5	10	0.6				
[Fe(TSPP)]-Zn_2Al-LDH	2	<1	8	0.7				
[Fe(TSPP)]-Zn_4Al-LDH	3	<1	5	0.6				
Fe(TDFSPP)[b]	4	42	<1	3.1	67	49	40	9.3
[Fe(TDFSPP)]-Zn_2Al-LDH	5	21	<1	1.3	10	37	20	8.8
Fe(TDCSPP)[b]	6	13	<1	0.7	62	100	82	31
[Fe(TDCSPP)]-Zn_2Al-LDH	7	21	<1	1.4	21	69	33	18
Zn_4Al-LDH[f]	8	<1	–		9.4	48	45	
Zn_2Al-LDH[f]	9	<1	–		8.3	25	18	
No catalyst solid[g]	10	<1	–		<1	15	6	
Final catalytic result[h]					Oxide (% yield)	One (% yield)	Ol (% yield)	
[Fe(TDFSPP)]-Zn_2Al-LDH [run 5 − (run 9 + run 10)]					2	–	–	
Fe(TDFSPP) [run 4 − run 10]					67	34	34	
[Fe(TDCSPP)]-Zn_2Al-LDH [run7 − (run 9 + run 10)]					13	34	9	
Fe(TDCSPP) [run 6 − run 10]					62	85	76	

[a] Typical reaction conditions: purged argon, catalyst/oxidant/cyclohexane molar ratio = 1:10:1000 mmol; solvent mixture dichloromethane/acetonitrile 1:1 (v/v) (350 μL) at room temperature (yields obtained after 1 h of reaction based on starting PhIO). It was assumed that two mols of PhIO are necessary for ketone formation.
[b] Homogeneous catalysis was carried out under identical conditions, in dichloromethane/acetonitrile 1:1 solvent mixture (v/v).
[c] Total yield of cyclohexanol.
[d] Total yield of cyclohexanone.
[e] Cyclohexene oxidation products: oxide = cyclohexane oxide (epoxide), one = 2-cyclohexen-1-one, ol = 2-cyclohexen-1-ol.
[f] Control reaction using Zn_nAl-LDH without FeP as catalyst in the same conditions as the oxidation reaction described in (a).
[g] Control reaction performed with PhIO and substrate without solid catalyst or FeP in solution.
[h] Final catalytic result is the yield % of each product from the cyclohexene oxidation after deducing the contribution of the product yields obtained from the control reactions (runs 9 and 10).
[i] TON = turnover number: mol of products/mol of catalyst.

Table 5
Conversion percentage of cyclohexene in the catalytic process involving iron porphyrins in solution and immobilized in LDH and the autooxidation reaction. Transformation of the final results in yield % based on PhIO

Catalyst system	Cyclohexene conversion (%)[a]			
	Run	Oxide	One	Ol
[Fe(TDFSPP)]-Zn_2Al-LDH + PhIO + substrate + solvent[b]	1	0.024	–	–
[Fe(TDFSPP)]-Zn_2Al-LDH + substrate + solvent[c]	2	–	0.0042	0.0063
Substrate + solvent[d]	3	0.00092	0.041	0.014
Final conversion result[e]		0.023	−0.045[f]	−0.020
	Yield (%)[g]			
[Fe(TDFSPP)]-Zn_2Al-LDH + PhIO + substrate + solvent[h]		1.9	–	–
Catalyst system	Cyclohexene conversion (%)[a]			
	Run	Oxide	One	Ol
Fe(TDFSPP)+ PhIO + substrate + solvent[b]	4	0.54	0.27	0.27
Fe(TDFSPP) + substrate + solvent[c]	5	0.029	0.88	0.38
Substrate + solvent[d]	3	0.00092	0.041	0.014
Final conversion result[e]		0.51	−0.65	−0.12
	Yield (%)[g]			
Fe(TDFSPP) + PhIO + substrate + solvent[h]		63	–	–

[a] The total mol of cyclohexene used was considered 100% conversion.
[b] Typical condition for run 1 was the same described in Table 3.
[c] Reaction performed without air control, in the same molar concentration and experimental conditions as run 1, in the absence of PhIO.
[d] Reaction performed in the same experimental condition of run 1 without air control, in the absence of PhIO and catalyst.
[e] % of cyclohexene conversion after deducing the results from the autooxidation routes [run 1 − (run 2 + run 3) in the case of heterogeneous catalysis and run 4 − (run 5 + run 6) for homogeneous catalysis.
[f] Negative results means that the autooxidation process, when there was no control of dioxygen conditions, leads to large and out of control conversion of cyclohexene to the allylic product.
[g] Yield % corrected: the results represent the tabled cyclohexene conversion results (oxide = 0.10%, one = 0.25%, and ol = 0.16%) now converted to the yield % based on the PhIO used in run 1 (heterogeneous catalysis) or run 4 (homogeneous catalysis), since all the reactions were performed in the same experimental conditions.
[h] % of cyclohexene conversion expressed as yields % (based on the PhIO) after all autooxidation processes are deduced.

products. This indicates that hydroxylation of cyclohexane can be attributed to the presence of the intercalated/adsorbed FeP only.

3.2.3. Cyclohexene

The products generated from cyclohexene oxidation mediated by PhIO/FeP systems result from a competition between the C=C

and allylic C–H groups on the alkene for the electrophilic active species, the ferryl porphyrin π-cation radical [45] generated in the reaction between FeP and iodosylbenzene. Oxidation of these groups should produce cyclohexenoxide and/or allylic alcohol (1-cyclohexen-3-ol) and ketone (1-cyclohexen-3-one), respectively [39,42,44]. Homogeneous FeP/PhIO systems lead to allylic products in minor yields compared with epoxide, and the efficiency and selectivity of the catalytic reaction toward the epoxide is controlled by the reaction conditions (solvent, temperature, inert atmosphere, and reactants molar ratio) [46], the structure of the porphyrin ring, and the presence of axial ligands to the iron center [33,37,46,47].

In a preliminary examination, the use of second-generation FePs in the oxidation of cyclohexene produced epoxide and significant yields of allylic oxidation products (runs 4–7 in Table 4). However, the control reactions indicated that the Zn_nAl-LDH support alone contributed greatly to the total product yields (runs 8 and 9 in Table 4), and that the reaction performed with PhIO and substrate only (run 10 in Table 4) also led to significant amounts of products. Therefore, the final product yields obtained after deducting the yields achieved in the control reactions (presented at the end of Table 4) should provide a more realistic picture of the catalytic results obtained with both homogeneous and intercalated FePs.

The product distributions and product yields achieved in the oxidation reactions catalyzed by the FePs are consistent with the presence of dioxygen in the reaction medium, especially in the case of the homogeneous second-generation FePs and the intercalated Fe(TDCSPP). Despite the argon purge carried out before the oxidation reaction, homogeneous catalysis probably promoted dioxygen solubilization throughout the reaction. Controlling the presence of dioxygen also is a problem inherent to heterogeneous catalysis, because this gas can be distributed in voids of small crystals of the Zn_nAl-LDH support, making it difficult to ensure the absence of this gas. The presence of dioxygen in the support was confirmed by the high yields of allylic products obtained when only the Zn_2Al-LDH support (with no intercalated FeP) was used as catalyst (run 9 in Table 4). The fact that [Fe(TDFSPP)]-Zn_2Al-LDH led to an epoxide yield of only 2% after correction confirms the low catalytic activity of this intercalated FeP compared with Fe(TDCSPP)-Zn_2Al-LDH, as was observed for the cyclohexane and cyclooctene substrates.

To gain insight into the contribution of the various oxidation routes to cyclohexene oxidation, we performed various experiments in the presence of dioxygen and absence of PhIO for both second-generation FeP systems. The results, expressed as the percentage of cyclohexene conversion to the reaction products, are given in Table 5 for Fe(TDFSPP). The same procedure also was carried out for Fe(TDCSPP), with similar results (not shown).

In fact, the oxidation of cyclohexene in the presence of FeP and air under magnetic stirring, under the same catalytic reaction conditions shown in Table 4 but without PhIO, resulted in preferable conversion of cyclohexene to allylic products, which is consistent with a free-radical autooxidation mechanism (heterogeneous catalysis, run 2; homogeneous catalysis, run 5 in Table 5) mediated by the FeP in solution or intercalated into Zn_nAl-LDH [48]. Most of the allylic products from cyclohexene conversion were produced when the substrate and solvent were stirred magnetically in air for the same period and at the same temperature as for the catalytic reaction (run 3 in Table 5). After considering all contributions from the autooxidation routes from the catalytic results and converting cyclohexene conversion % into yield %, only epoxide yields were obtained for both the homogeneous and heterogeneous Fe(TDFSPP) catalysts (homogeneous catalysis, 63% epoxide yield; heterogeneous catalysis, 1.9% epoxide yield). For the homogeneous Fe(TDCSPP), the epoxide yield was 61% and the yield of allylic products was >50%. For the heterogeneous Fe(TDCSPP), an epoxide yield of 13% and an allylic product yield of 36% (29% ketone and 7% alcohol) were obtained. These results corroborate the results described above for the other two substrates (cyclohexane and cyclooctene); the heterogeneous catalyst led to lower yields than those achieved with the homogeneous counterparts, due to steric constraints on the access of the oxidant and reagent to the active site of the intercalated catalyst. In homogeneous medium, the two anionic second-generation FePs displayed similar catalytic behavior, leading to preferable epoxide formation. This is because both active species were electron-deficient, due to the presence of halogen atoms. Despite the fact that we could not control all of the autooxidation routes so as to know the exact amount of allylic products that they generated, the approximate final yield % results given in Table 5 suggest that Fe(TDFSPP) was even more selective toward the epoxide than Fe(TDCSPP) in the conditions used here. This may be related to the different electron-deficiency imposed by the halogen atoms fluorine and chlorine on the structures of the anionic FeP rings. The presence of these electron-withdrawing groups in the periphery of the porphyrin rings make the catalytic species more electrophilic, and thus more reactive, toward the electron-rich C=C bond. Because the fluorine atoms are more electronegative than chlorine, the active species generated from the reaction between Fe(TDFSPP) and PhIO is more reactive toward the C=C bond, leading to higher selectivity toward the epoxide [46].

In summary, the catalytic results obtained from cyclohexane oxidation reactions give evidence that both second-generation FePs are catalytically active in homogeneous solution and when intercalated into Zn_nAl-LDH. Interestingly, the catalytic results depend on the particular features of the porphyrin ring structures. Research using other substrates, such as linear alkanes, is currently underway in our laboratory, as is an investigation of the kinetic behavior of these catalysts.

4. Conclusion

First- and second-generation tetraanionic porphyrins and iron(III) porphyrins were successfully intercalated between Zn_nAl-LDH layers for the first time, using coprecipitation reaction at constant pH. The intercalation process seemed to favor the catalytic activity of Fe(TDCSPP), probably because the supported catalyst was less susceptible to inactivation by molecular aggregation and/or bimolecular self-destruction than the parent FeP in solution. The inverse behavior was observed with Fe(TDFSPP), suggesting that steric hindrance to the access of the oxidant and substrate to the active site of the intercalated FeP should be considered during the design of immobilized catalysts, especially when intercalated molecules are involved.

Acknowledgments

Financial support was provided by the Coordenação de Aperfeiçoamento de Pessoal de Nível Superior (CAPES) and Conselho Nacional de Desenvolvimento Científico e Tecnológico (CNPq). The authors also thank the Fundação Araucária, Fundação da Universidade Federal do Paraná (FUNPAR), Universidade Federal do Paraná (UFPR), Laboratoire des Matériaux Inorganiques (LMI), Centre National de la Recherche Scientifique (CNRS), and Université Blaise Pascal for support and assistance.

References

[1] D. Mansuy, C. R. Chim. 10 (2007) 1.
[2] S. Nakagaki, K.A.D.F. Castro, G.S. Machado, M. Halma, S.M. Drechsel, F. Wypych, J. Braz. Chem. Soc. 17 (2006) 1672.
[3] J.D. Harvey, C.J. Zeigler, J. Inorg. Biochem. 100 (2006) 869.
[4] F. Bedioui, Coord. Chem. Rev. 144 (1995) 39.
[5] J. Haber, L. Matachowski, K. Pamin, J. Poltowicz, J. Mol. Catal. A Chem. 198 (2003) 215.

[6] M. Halma, A. Bail, F. Wypych, S. Nakagaki, J. Mol. Catal. A Chem. 243 (2006) 44.
[7] F.L. Benedito, S. Nakagaki, A.A. Saczk, P.G. Peralta-Zamora, M.C.M. Costa, Appl. Catal. A Gen. 250 (2003) 1.
[8] Y. Iamamoto, Y.M. Idemori, S. Nakagaki, J. Mol. Catal. A Chem. 99 (1985) 187.
[9] M.A. Matinez-Lorente, P. Battioni, W. Kleemiss, J.F. Bartoli, D. Mansuy, J. Mol. Catal. A Chem. 113 (1996) 344.
[10] S. Nakagaki, C.R. Xavier, A.J. Wosniak, A.S. Mangrich, F. Wypych, M. Cantão, I. Denicoló, L.T. Kubota, Colloids Surf. A 168 (2000) 261.
[11] N. Herron, J. Coord. Chem. Soc. 19 (1998) 25.
[12] P. Battioni, R. Iwanejko, D. Mansuy, T. Mlodnicka, J. Poltowicz, F. Chanchez, J. Mol. Catal. A Chem. 109 (1996) 91.
[13] L. Barloy, J.P. Lallier, P. Battioni, D. Mansuy, Y. Pitfard, M. Tournoux, J.B. Valim, W. Jones, New J. Chem. 16 (1992) 71.
[14] A.M. Machado, F. Wypych, S.M. Drechsel, S. Nakagaki, J. Colloid Interface Sci. 254 (2002) 158.
[15] S. Nakagaki, M. Halma, A. Bail, G.G.C. Arízaga, F. Wypych, J. Colloid Interface Sci. 281 (2005) 417.
[16] F. Wypych, G.A. Budniak, M. Halma, S. Nakagaki, J. Colloid Interface Sci. 264 (2003) 203.
[17] S. Bonnet, C. Forano, A. Roy, J.P. Besse, P. Maillard, M. Momenteau, Chem. Mat. 8 (1996) 1962.
[18] M. Halma, F. Wypych, S.M. Dreschel, S. Nakagaki, J. Porph. Phthal. 6 (2002) 502.
[19] Z. Tong, T. Shichi, G. Zhang, K. Takagi, Res. Chem. Intermed. 29 (2003) 335.
[20] F. Wypych, A. Bail, M. Halma, S. Nakagaki, J. Catal. 234 (2005) 431.
[21] S. Nakagaki, G.S. Machado, M. Halma, A.A.S. Marangon, K.A.D.F. Castro, N. Mattoso, F. Wypych, J. Catal. 242 (2006) 110.
[22] S.S. Cady, T. Pinnavaia, J. Inorg. Chem. 17 (1978) 1501.
[23] M. Chibwe, L. Ukrainczyk, S.A. Boyd, T.J. Pinnavaia, J. Mol. Catal. A Chem. 249 (1996) 113.
[24] S. Nakagaki, A.R. Ramos, F.L. Benedito, P.G. Peralta-Zamora, A.J.G. Zarbin, J. Mol. Catal. A Chem. 185 (2002) 203.
[25] S. Nakagaki, F.L. Benedito, F. Wypych, J. Mol. Catal. A Chem. 17 (2004) 121.
[26] D. Dolphin, T.G. Traylor, L.Y. Xie, Acc. Chem. Res. 30 (1997) 251.
[27] T. Hibino, W. Jones, J. Mater. Chem. 11 (2001) 1321.
[28] H. Turk, W.T. Ford, J. Org. Chem. 511 (1991) 253.
[29] J.S. Lyndsey, I.C. Schreiman, H.C. Hsu, P.C. Kearney, A.M. Marguerettaz, J. Org. Chem. 52 (1987) 827.
[30] A. Adler, F.R. Longo, J. Am. Chem. Soc. 86 (1964) 3145.
[31] A. Adler, F.R. Longo, F. Kampas, J. Kim, Inorg. Nucl. Chem. 32 (1979) 2443.
[32] J.G. Sharefkin, H. Saltzmann, Org. Synth. 43 (1963) 62.
[33] H.J. Lucas, E.R. Kennedy, M.W. Forno, Org. Synth. 43 (1963) 483.
[34] J. Rodriguez-Carvajal, Newslet. Powder Diff. Comm. Int. Un. Crystall. 26 (2001) 12.
[35] A. Ennadi, A. Legrouri, A. Roy, J.P. Besse, J. Mater. Chem. 10 (2000) 2337.
[36] CS Chem3D Ultra Program—Cambridge Soft Corporation, CS Chem3D Ultra 5.0: Ultimate Modeling, Visualization and Analysis, Cambridge, 1998.
[37] Z. Chang, D.G. Evans, C. Vial, J. Ghanbaja, V. Prévot, M. Roy, C. Forano, J. Solid State Chem. 178 (2005) 2766.
[38] K. Nakamoto, Infrared and Raman Spectra of Inorganic and Coordination Compounds, fifth ed., Wiley, New York, 1997, pp. 263, 324.
[39] A.J. Appleton, S. Evans, J.R. Lindsay Smith, J. Chem. Soc. Perkin Trans. 2 (1995) 28.
[40] J.T. Groves, T.E. Nemo, R.S. Meyers, J. Am. Chem. Soc. 101 (1979) 1032.
[41] J.T. Groves, R.C. Haushalter, M. Nakamura, T.E. Nemo, B.J. Evans, J. Am. Chem. Soc. 103 (1981) 2884.
[42] J.T. Groves, J. Inorg. Biochem. 100 (2006) 434.
[43] T. Kamachi, T. Kouno, W. Nam, K. Yoshizawa, J. Inorg. Biochem. 100 (2006) 751.
[44] J.T. Groves, T.E. Nemo, J. Am. Chem. Soc. 105 (1983) 5786.
[45] J.T. Groves, J. Inorg. Biochem. 110 (2006) 434.
[46] W.J. Song, Y.O. Ryu, R. Song, W. Nam, J. Biol. Inorg. Chem. 10 (2005) 294.
[47] J.A. Smegal, C.L. Hill, J. Am. Chem. Soc. 105 (1983) 3515.
[48] D. Paulson, R. Ullman, R.B. Sloane, J. C. S. Chem. Commun. (1984) 186.